Journal of Alloys and Compounds 509 (2011) 9742–9752

Contents lists available at ScienceDirect

Journal of Alloys and Compounds

journal homepage: www.elsevier.com/locate/jallcom

First principles study of the electronic and magnetic properties of semi-Heusler alloys NiXSb (X = Ti, V, Cr and Mn)

M.P. Ghimire[a,b,*], Sandeep[c], T.P. Sinha[d], R.K. Thapa[c]

[a] Faculty of Science, Nepal Academy of Science and Technology, G.P.O. 3323, Kathmandu, Nepal
[b] Condensed Matter Physics Research Center, Butwal, Rupandehi, Nepal
[c] Department of Physics, Mizoram University, Aizawl 796009, Mizoram, India
[d] Department of Physics, Bose Institute, 93/1, A.P.C. Road, Kolkata 700009, India

ARTICLE INFO

Article history:
Received 26 June 2011
Received in revised form 1 August 2011
Accepted 4 August 2011
Available online 11 August 2011

Keywords:
Semi-Heusler alloys
Electronic and magnetic structure
DFT
FP-LAPW
Half-metallic ferromagnetism

ABSTRACT

The electronic density of states (DOS), magnetic moments and band structure of semi-Heusler alloy NiXSb (where X = Ti, V, Cr and Mn) has been studied by using the first principles full-potential linearized augmented plane wave method (FP-LAPW) based on density functional theory (DFT). For the exchange and correlation potential generalized-gradient approximation (GGA) is used. From the observations, NiTiSb shows the possibility of half-metallic ferromagnet (HMF) behavior with a band gap of 0.53 eV and an effective moment of 0.35 μ_B. The alloys like NiVSb, NiCrSb and NiMnSb are HMF with band gap of 0.49 eV, 0.38 eV and 0.48 eV and an effective moment of 1.995 μ_B, 3.01 μ_B and 3.99 μ_B respectively. DOS and band structure result shows the 3d states of Ni overlap with 3d states of X atoms suggesting hybridization between them. The exchange-splitting of Ni-3d and X-3d state electrons lead to localized spin moment which determines the HMF behavior of NiXSb. The results obtained are compared and found to be in close agreement with the available data.

1. Introduction

The concept of half-metallic ferromagnets (HMF) was introduced by de Groot and Bushow [1] on the basis of band structure calculations in NiMnSb. Due to ferromagnetic (FM) decoupling, spin-up bands are metallic and spin-down bands are semiconducting or vice versa. The inter-metallic systems like NiXSb (where X are transition metals such as V, Cr and Mn) with space group *F43m* are half metals (HM) with energy gap in spin-down channel. From the definition of half-metals, the spin polarization of electrons is 100% at the Fermi level (E_F), which is confirmed experimentally with spin-resolved photoemission [2]. For HM, one spin channel has a large DOS exhibiting the metallic Fermi cut-off whereas the other spin channel shows a vanishing DOS with band gap at E_F [3]. They are also revealed by the clear separation of antibonding spin-up states which cross E_F from the antibonding spin-down states which are separated by a gap almost equal to the exchange energy. HMF are widely applicable in non-volatile magnetic random access memories (MRAMs), opto-electronic devices etc. They are expected to provide huge tunnel magneto-resistance (TMR) and giant magneto-resistance (GMR) in magneto-electronic devices. They are also used as perfect spin filters and spin-injection devices as an alternative to FM 3d metals [4,5].

Several authors had studied the electronic and magnetic properties of semi-Heusler alloys. de Groot and Bushow [1] and Kubler [6] recognized that the electronic structure and hence the properties of the Heusler compounds are very sensitive to the valence electron count (VEC) [7]. Jung et al. [8] suggested that the 19 electrons of NiTiSb would undergo Stoner instability [9] to a FM ground state. They also explained that 18 electron compounds are non-magnetic and semi-conducting while the 22 electron compounds (like NiMnSb) are localized moment ferromagnets. Galanakis et al. [10] placed the 18 electron rule on a more formal footing which supports the earlier works of Jung et al. [8]. The importance of VEC in semi-Heusler compounds was first recognized by Pierre et al. [11]. They described the transport and magnetic properties of various phases of semi-Heusler alloys which arise from the particular crystallographic structure and narrow band phenomena. Tabola and Pierre [12] have emphasized on the importance of covalency in semi-Heusler compounds using the Korringa–Kohn–Rostoker (KKR) computations within the LDA framework. Ogut and Rabe [13] have examined the electronic structures of XNiSn (where X = Ti, Zr and Hf), and interpreted their nature of band gaps. Nanda and Dasgupta [14,15] have examined nearly 20 different $C1_b$ compounds

* Corresponding author at: Faculty of Science, Nepal Academy of Science and Technology, G.P.O. 3323, Kathmandu, Nepal. Tel.: +977 1 5547715; fax: +977 1 5547713.
E-mail address: ghimire.mpg@gmail.com (M.P. Ghimire).

0925-8388/$ – see front matter © 2011 Elsevier B.V. All rights reserved.
doi:10.1016/j.jallcom.2011.08.017

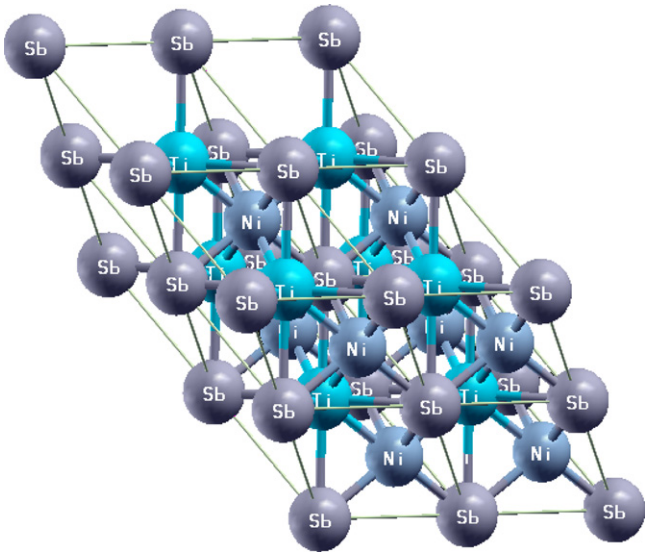

Fig. 1. The crystal structure of NiTiSb which is representative of the general structure observed in NiXSb semi-Heusler alloys in zinc-blende structure.

using the tight binding full-potential linear muffin-tin orbital (FP-LMTO) and tight-binding linear muffin-tin orbital method in the atomic sphere approximation (LMTO-ASA) methods, including a detailed analysis of the bonding and the nature of band gaps. They ascribed HMF to arise in some of the $C1_b$ compounds due to the large X-Sb covalency, in conjunction with large exchange-splitting due to highly magnetic X ions (where X = transition metals like Ni). Zhang et al. [16,17] had used the FP-LAPW method within local-spin density approximation (LSDA) to search for new HMF's in semi-Heusler alloys NiVM and NiCrM (where M = P, As, Sb, S, Se and Te). They found that NiVAs, NiCrP, NiCrSe and NiCrTe are HMF's while NiVP and NiVSb are nearly HMF's. Li and Jin [18] also studied the XYZ semi-Heusler alloys (where X = Mn, Ni; Y = Cr, Mn; Z = As, Sb) by using the FP-LAPW method within GGA to predict their electronic structures. They observed that NiCrSb is almost a HMF.

We present here the first principles calculation of the electronic and magnetic properties of NiXSb using FP-LAPW based GGA method in the framework of DFT [19]. We found that the present calculations are more consistent to predict the HMF's of semi-Heusler alloys. For computing the DOS, magnetic moments and band structures, WIEN2k code [20] is used.

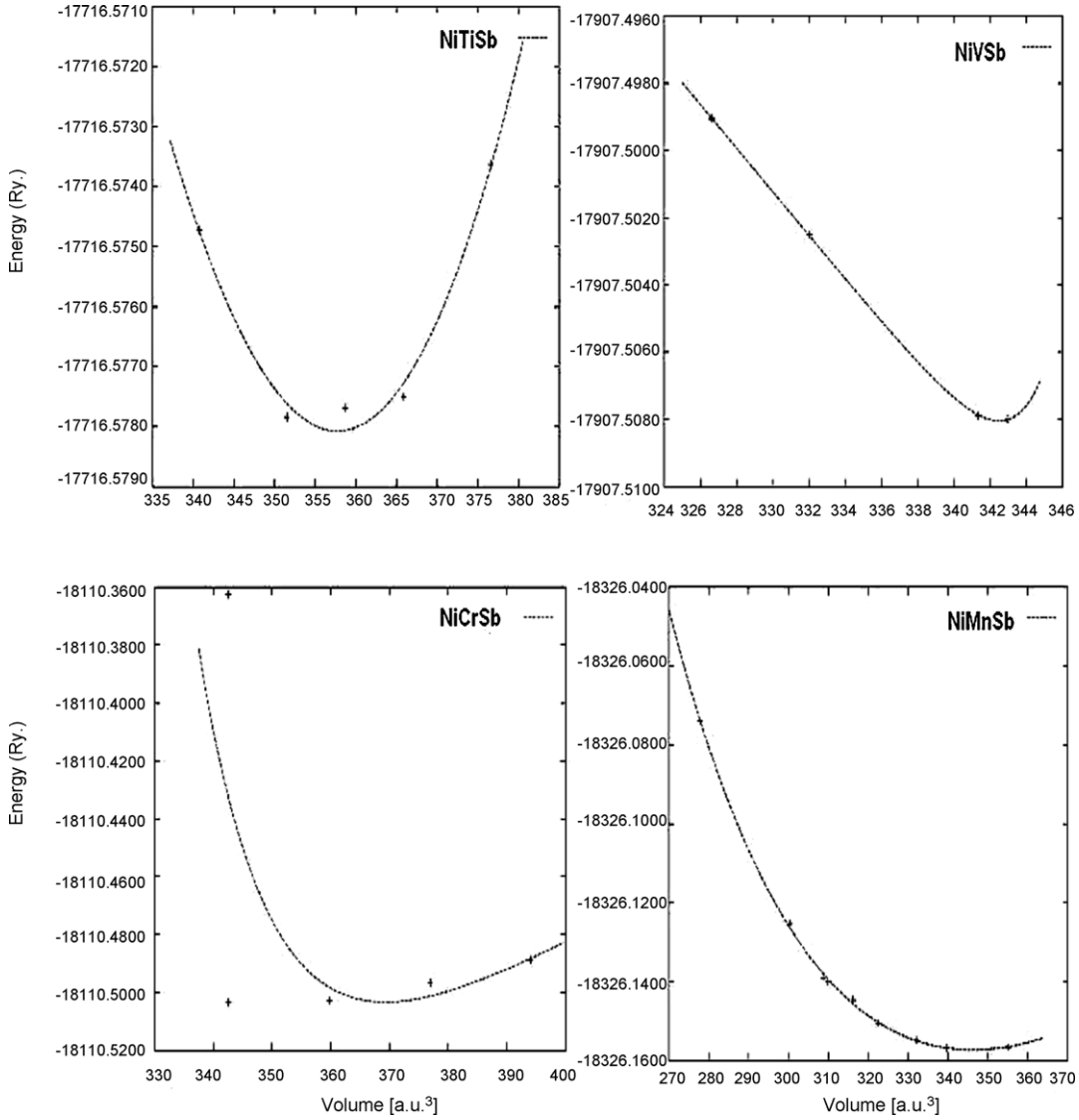

Fig. 2. Energy vs volume curve for obtaining the optimized lattice parameters of NiXSb by volume optimization method.

Table 1
Calculated results of the optimized lattice parameters a_0, compared lattice parameters a, bulk pressure (B), pressure derivative (B') and the ground state energy (E) of NiTiSb, NiVSb, NiCrSb and NiMnSb.

NiXSb	a_o (Å)	a (Å)	B (GPA)	B'	Energy (Ry)
NiTiSb	5.964	5.87 [23]	125.20	−3.31	−17716.58
NiVSb	5.79	5.89 [17]	1600.78	−167.47	−17907.51
NiCrSb	6.025	5.96 [18]	460.37	27.82	−18110.50
NiMnSb	5.897	5.93 [1]	107.99	5.66	−18326.16

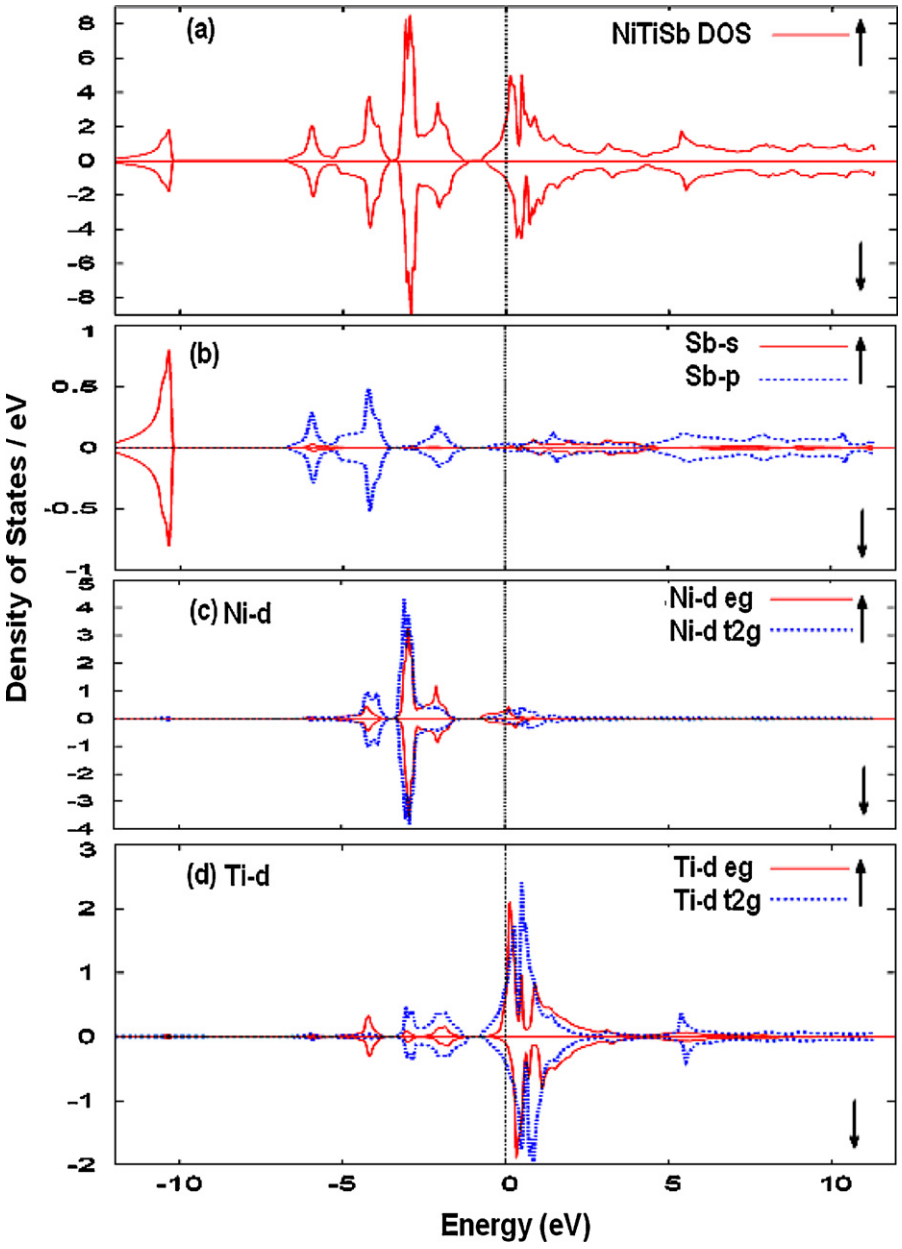

Fig. 3. The spin-dependent total DOS of NiTiSb and partial DOS of Sb-s,p, Ni-d and Ti-d states.

Table 2
The spin resolved and l-decomposed density of states at the Fermi energy for NiXSb in states/eV/formula unit (where X = Ti, V, Cr and Mn).

NiXSb	Ni-d	Mn-d	Sb-p	Total DOS
NiTiSb (up)	0.4	1.4	0.08	3.2
NiTiSb (down)	0.2	0.5	0.06	1.3
NiVSb	0.3	1.6	0.05	3.1
NiCrSb	0.35	0.5	0.08	2.1
NiMnSb	0.2	0.3	0.07	0.71

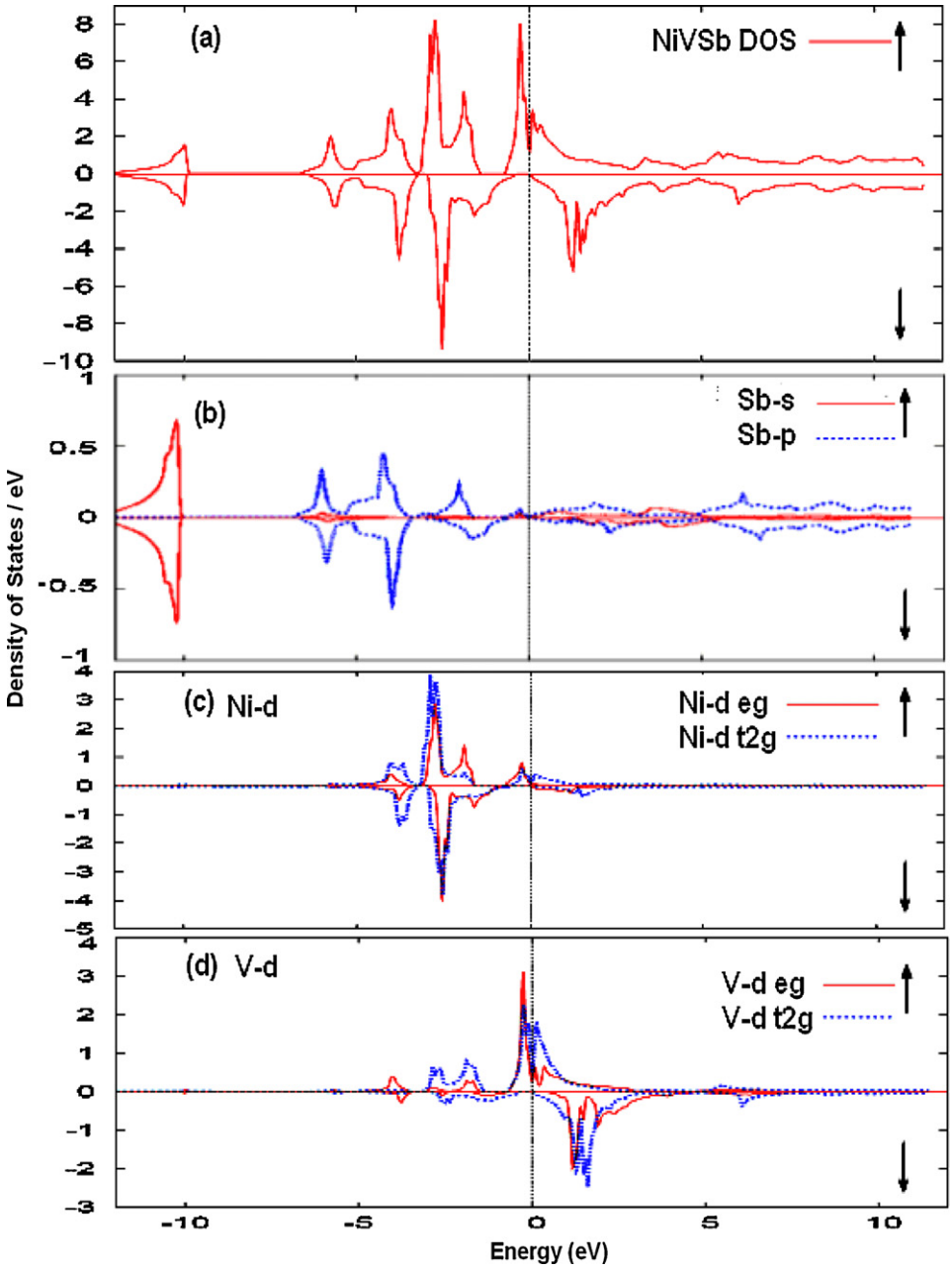

Fig. 4. The spin-dependent total DOS of NiVSb and partial DOS of Sb-s,p, Ni-d and V-d states.

2. Crystal structure and computational details

The inter-metallic compound NiXSb (where X = Ti, V, Cr and Mn) with space group *F43m* crystallizes in a cubic structure of MgAgAs type with the *f.c.c.* bravais lattice with one formula unit per unit cell as shown in Fig. 1. We considered the standard representation of $C1_b$ structure with *f.c.c.* unit cell containing three atoms: X (0, 0, 0), Sb (1/2, 1/2, 1/2), Ni (1/4, 1/4, 1/4), and a vacant site at (3/4, 3/4, 3/4) [14].

In this work FP-LAPW method have been applied to perform first principles total energy calculations. This method is based on DFT which is a universal quantum mechanical approach for many body problems [19]. To take into account the exchange and correlation effects, GGA as parametrized by Perdew et al. [21] has been used. We have chosen the muffin-tin (MT) radii for Ni, Ti, V, Cr, Mn and Sb to be 2.41, 2.35, 2.37, 2.39, 2.41 and 2.27 a.u. respectively. Integrations in reciprocal space were performed using 504 spatial *k*-points in the irreducible wedge of the BZ. The value for the convergence parameters are taken to be $R_{MT} \times K_{MAX} = 7$ which controls the size of the basis sets consisting of the plane waves. G_{MAX} is chosen to be 12 (a.u.)$^{-1}$ for consistency. Convergence is achieved with energy tolerance of 10^{-3} Ry. The ground state electronic structures of these materials are calculated by using the optimum value of the lattice parameters. To obtain the optimum value of the lattice parameters, we have calculated the ground state total energies for different volumes ranging between −10 and +10% of the experimental (theoretical) lattice parameters. The calculated results are fitted to the Murnaghan equation of state [22] defined by

$$E(V) = E_0 + \frac{B_0 V}{B_0'}\left[\frac{(V_0/V)^{B_0'}}{B_0' - 1} + 1\right] - \frac{B_0 V_0}{B_0' - 1},$$

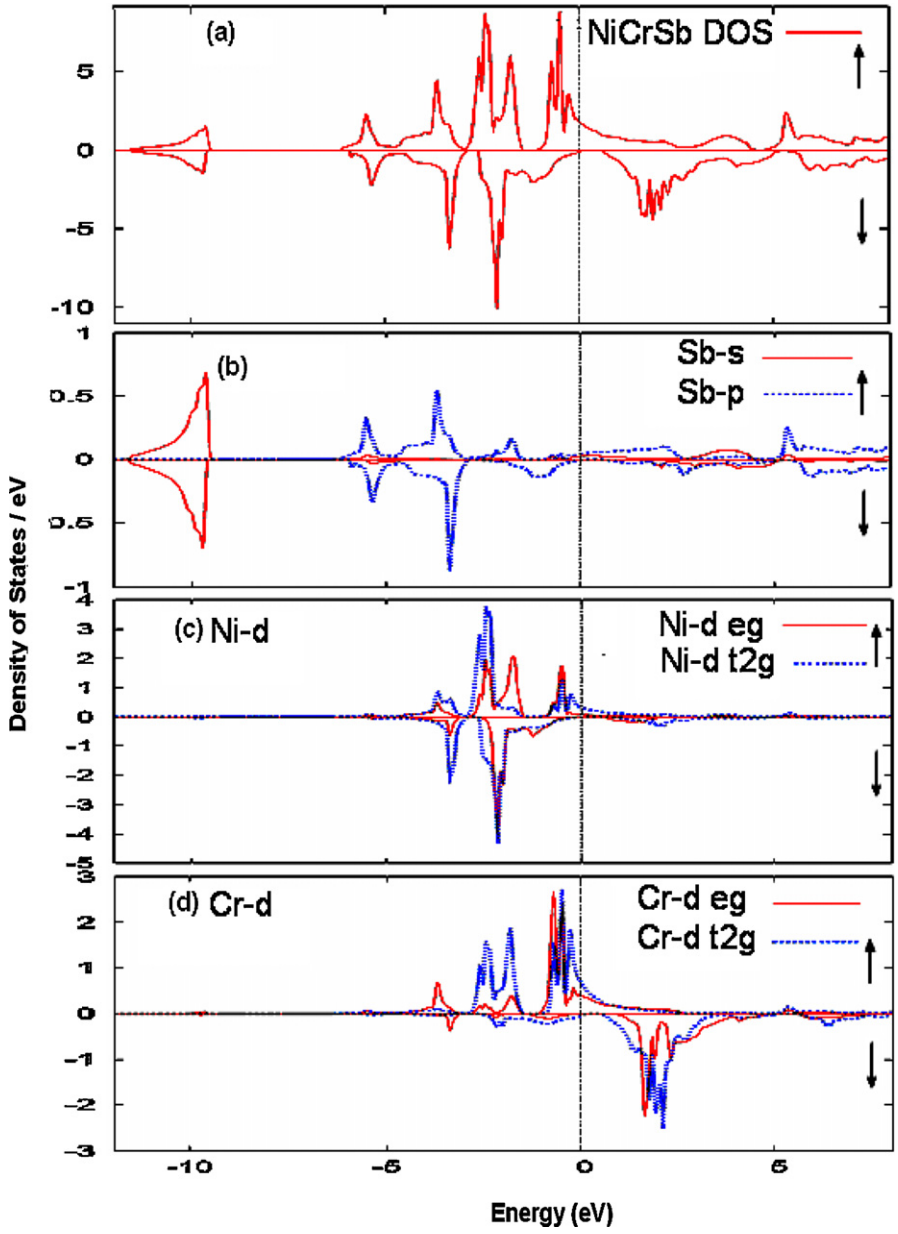

Fig. 5. The spin-dependent total DOS of NiCrSb and partial DOS of Sb-s,p, Ni-d and Cr-d states.

where V_0 is the equilibrium volume and B_0 is the bulk modulus given by $B_0 = -V(\delta P/\delta V)_T$ evaluated at volume V_0. B_0' is the pressure derivative of B_0 evaluated at volume V_0.

3. Results and discussions

3.1. Structural optimization

Within the FP-LAPW scheme, structural optimization is performed for NiXSb alloys to find their lattice parameters resulting in minimum of the total energy. The optimized volume vs energy curve is shown in Fig. 2. The optimized lattice parameters, pressure, pressure derivative and minimum ground state energy are given in Table 1 along with the experimental and theoretical lattice parameters for comparison [1,17,18,23]. From Fig. 2, it can be observed that the increase in lattice parameter shows the decrease in bulk pressure and hence increase in the pressure derivatives for 3d based semi-Heusler alloys. The optimized lattice parameters of NiTiSb, NiVSb and NiCrSb are found to be 2%, 0.09% and 0.7% larger than the compared values while for NiMnSb, it is 0.6% smaller.

3.2. Density of states

The total DOS of NiXSb along with the partial DOS of Ni-d, X-d and Sb-s,p for spin-up and spin-down configurations are shown in Figs. 3–6. The maximum total DOS contributions at E_F in states/eV were found to be 3.2, 2.9, 2.1 and 0.71 respectively for NiTiSb, NiVSb, NiCrSb and NiMnSb in spin-up configuration. Table 2 shows the principal character of NiXSb electrons at E_F due to Ni-d, Sb-p and X-d along with their total DOS.

From the total and partial DOS plots of NiXSb in spin-up and spin-down configurations, it is observed for all systems that Sb-s states are contributing in the core region while Sb-p states are contributing in the semi-core and the valence region. Observation showed that when moving from NiTiSb to NiMnSb, the crystal field splitting as well as the exchange energy splitting increases. This behavior of increasing in exchange energy shows the increasing

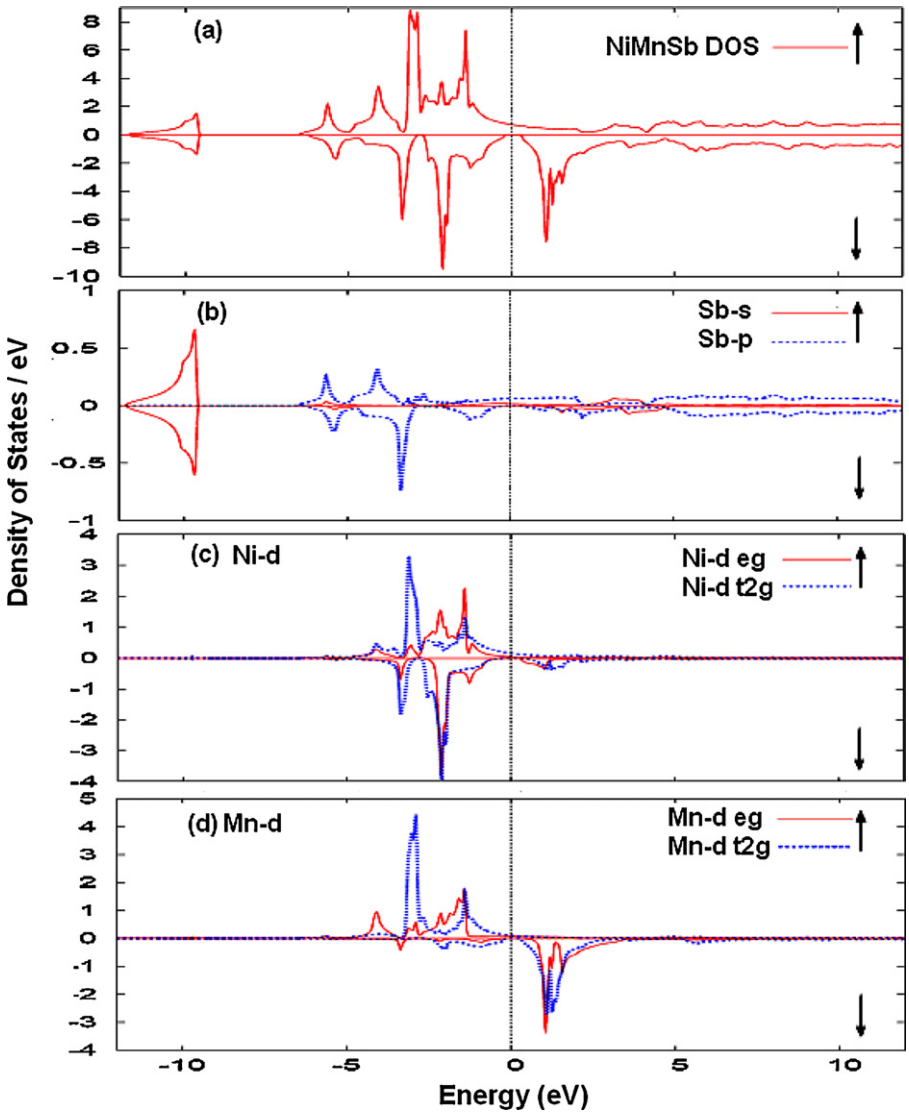

Fig. 6. The spin-dependent total DOS of NiMnSb and partial DOS of Sb-s,p, Ni-d and Mn-d states.

magnetic moment and hence its FM behavior. From the DOS plots (partial and total) we observe a shift of the Fermi level in NiXSb (X = Ti, V and Cr) when compared with NiMnSb. Therefore, the X-d states are found to be mainly responsible for the FM state of NiXSb due to their exchange splittings. For all these systems except NiTiSb, spin-up DOS shows the metallic behavior with Fermi cut-off while spin-down shows a band gap at E_F showing the semi-conducting behavior.

From the DOS plot of NiTiSb as shown in Fig. 3 it is observed that spin-up and spin-down channel shows a semi-conducting behavior

Table 3
Calculated results of equilibrium lattice parameters a_o, energy band gaps (E_g) and the individual and total magnetic moments (m) for NiXSb (where X = Ti, V, Cr and Mn).

NiXSb	a_o (Å)	Band gap, E_g (eV)	Magnetic moment, m (μ_B)		
			X	Ni	Total
NiTiSb	5.96	0.53	0.27	0.01	0.35
	5.87 [23]	0.5 [12,25]	–	–	0.02 [23]
NiVSb	5.79	0.49	1.745	0.25	1.99
	5.89 [17]	0.33 [17]	1.85 [17]	0.11 [17]	1.90 [17]
	5.79 [27]	0.52 [27]	–	–	1.99 [27]
NiCrSb	6.0	0.38	2.99	0.02	3.01
	5.86 [16]	–	2.99 [16]	0.047 [16]	2.918 [16]
	5.96 [18]	0.31 [18]	2.92 [18]	0.03 [18]	3. 05 [18]
NiMnSb	5.897	0.48	3.73	0.25	3.99
	5.93 [27]	0.49 [27]	–	–	3.97 [27]
	5.93 [1]	0.55 [30]	3.76 [30]	0.26 [30]	3.85 [31]
	–	–	–	–	3.99 [32]

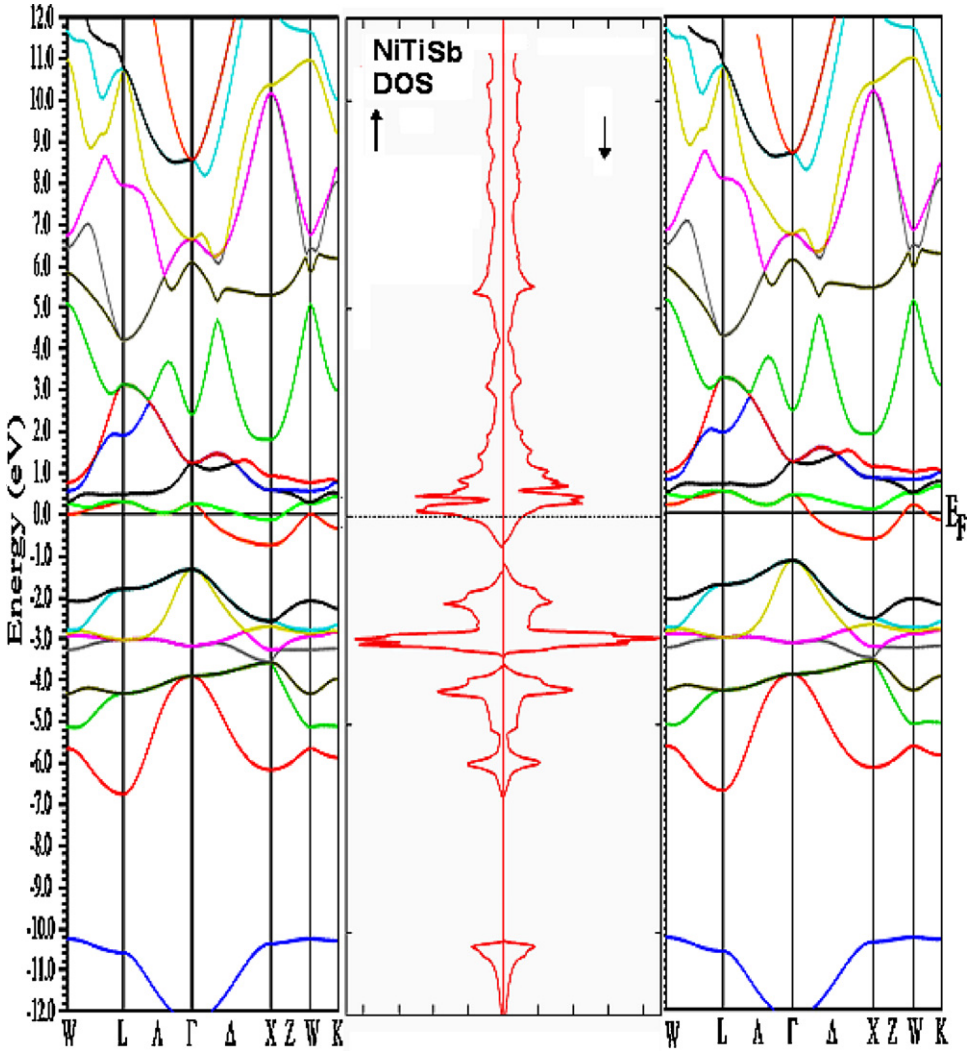

Fig. 7. Band structure in spin-up (left), spin-down (right) and DOS (middle) plots for NiTiSb. The horizontal line on the plot corresponds to the Fermi level.

with energy gap of 0.53 eV just below E_F. Sharp peaks are observed in the valence and the conduction region of both spin channels. A small hybridization between Ni-3d and Ti-3d states is observed at E_F. Studies of Nanda and Dasgupta [14,15] had reported a similar DOS in their FP-LMTO and LMTO-ASA results. We observed a similar DOS profile with little variation in band gap when compared with the results of Ishida et al. [24] and Tobola et al. [25]. Due to the crystal field splitting, the d-states of Ni and Ti splits into t_{2g} and e_g states. The t_{2g} state lies in the lower energy side whereas e_g lies in higher energy side. Exchange splitting between spin-up and down states of Ti-d-e_g is observed with exchange energy of 0.2 eV while the exchange splitting due to Ni-d states is negligible. The splitting in d states of Ti and Ni give rise to small FM behavior of NiTiSb. This is because the Fermi level is at the anti-bonding complex of predominantly Ti character with gap below E_F. Further, the depletion of the spin-down anti-bonding states above the gap may happen such that none of the spin-down anti-bonding states are occupied resulting into a complete spin polarization [26,27]. Hence, there is possibility of HMF in NiTiSb.

For the case of NiVSb as shown in Fig. 4, the total DOS plots of spin-up shows a sharp peak near E_F in the valence region while in spin-down, the peak lies in the conduction region. These contributions in both spin channels are due to V-d states weakly hybridized with the Ni-d states. An energy gap of 0.49 eV is observed for NiVSb in spin-down channel showing half-metallicity to the system [26,28]. The result observed agrees well with the results of Nanda and Dasgupta [14] and Kandpal et al. [27] but not consistent with the results of Zhang et al. [17]. They observed it to be nearly half-metallic.

From the DOS plot of NiCrSb as shown in Fig. 5, strong hybridization is observed between Ni-d and Cr-d electrons below E_F in both spin channels while in the conduction region no such characteristics are observed. Like NiVSb, spin-up channel shows the metallic behavior and spin-down shows the semi-conducting behavior with an energy gap of 0.38 eV. The system NiCrSb therefore acts as a half-metal. Unlike the present calculations, Zhang et al. [16] observed nearly HM behavior with a band gap of 0.26 eV.

The DOS plot of NiMnSb is shown in Fig. 6. As in NiVSb and NiCrSb, we observe the metallic behavior for spin-up and semi-conducting behavior for spin-down configurations in NiMnSb. Thus, it behaves as a half-metal with band gap of 0.48 eV. In spin-up state, the main contribution in valence band region comes from the d-states of Ni and Mn which hybridized with the p-state of antimony. It is observed that Sb-s states are mostly contributing to the total DOS in the core region while its p-states is contributing in the semi-core and the valence region in both spin channels. In the conduction region, there is a small contribution from Sb-p state in spin-up whereas Mn-d states have the dominating role in spin-down. The conduction region shows no peaks in the spin-up channel. Strong hybridization between Ni-3d and Mn-3d state

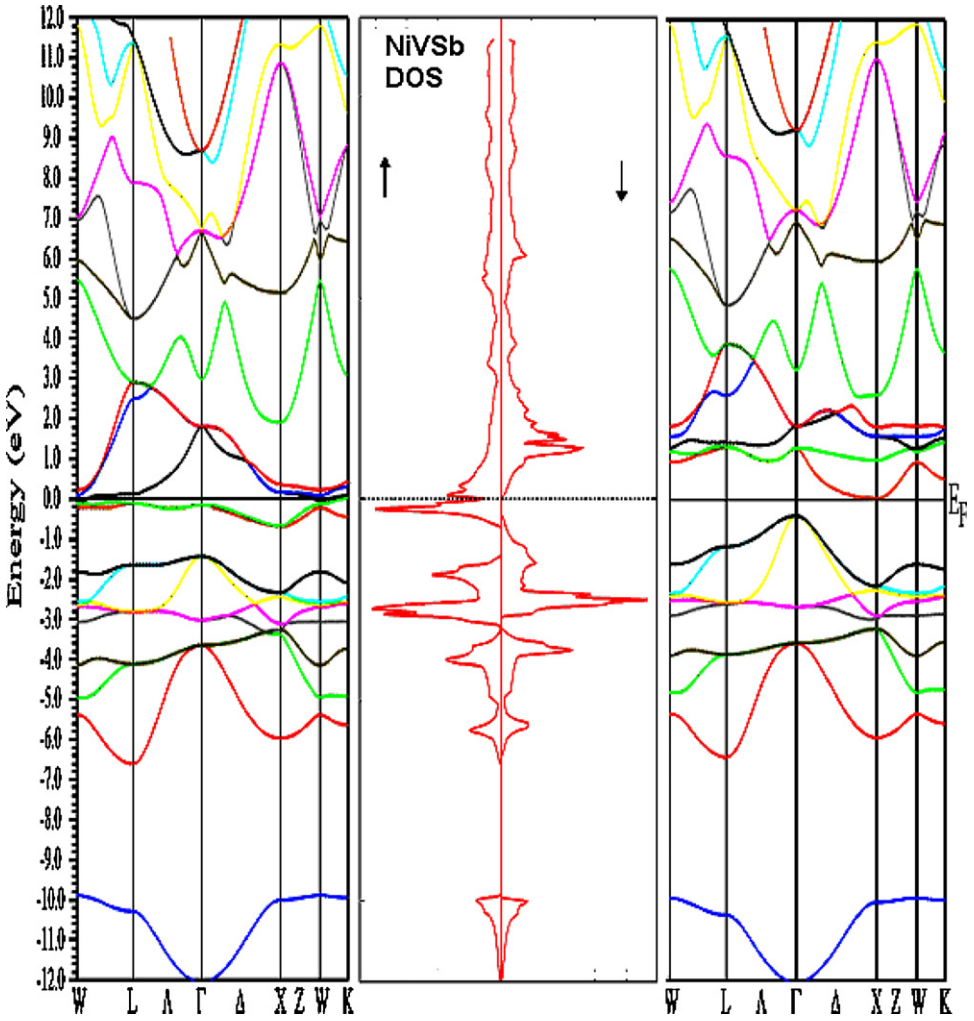

Fig. 8. Band structure in spin-up (left), spin-down (right) and DOS (middle) plots for NiVSb. The horizontal line on the plot corresponds to the Fermi level.

electrons is found to occur below and above E_F in the spin-up channel. Our observation showed that Nanda and Dasgupta [14,15] under-estimated the band gap in NiMnSb with the FP-LMTO and LMTO-ASA method. The d-states of Ni and Mn splits into t_{2g} and e_g states due to crystal field splitting. The crystal field splitting energy for Ni and Mn in spin-up is found to be 2.0 eV and 1.8 eV respectively. In spin-down configuration, the crystal field splitting energy for Ni and Mn is 1.5 eV and 0.5 eV respectively. The exchange splitting energy for Ni-e_g state is 0.5 eV and for t_{2g} state it is 0.2 eV. Similarly, the exchange energy for Mn-e_g is 2.5 eV and t_{2g} state is 3.1 eV. Such value of exchange splitting shows the magnetic behavior of Ni and Mn in NiMnSb. For Ni, it is observed that the t_{2g} and e_g state are filled in both spin channels and therefore lies in the valence band region whereas for Mn, t_{2g} and e_g states are completely filled in spin-up channel but in spin-down, they are completely vacant and thus lies in the conduction region. This indicates that Mn is in high spin configuration with 2^+ states in NiMnSb.

3.3. Magnetic moments

In HMF compounds all states of one spin valence band are occupied and thus their total number is an integer and their total magnetic moment is also an integer [29]. We have compared the moment of NiXSb with earlier results and were found to support the HMF nature of NiVSb, NiCrSb and NiMnSb while for NiTiSb, nearly HMF behavior is observed. For the semi-Heusler alloys, the moments due to 3d states of Ni, Ti, V, Cr and Mn are contributing to the effective moment of the systems. Table 3 summarizes the effective and individual spin moments of NiTiSb, NiVSb, NiCrSb and NiMnSb respectively.

From the DOS plots of NiXSb, we observe the exchange splitting effects between e_g (t_{2g}) up and e_g (t_{2g}) down for Ni and X atoms. This exchange splitting between the d-state electrons of Ni and X atom give rise to the magnetic behavior of the compounds. The magnetic moment of NiTiSb is found to be 0.35 μ_B which is slightly higher than the results obtained by Kandpal [23]. He also observed NiTiSb to be nearly HMF with a moment of 0.02 μ_B. Our observed value of the moment for NiTiSb shows indication of HMF depending on the interpretation of Stoner's stability [9].

Similar characteristic of the magnetic moments is observed for NiVSb, NiCrSb and NiMnSb. The effective magnetic moment of NiVSb we obtained is 2.0 μ_B which confirms the HMF's behavior. The obtained result is found to be more consistent with the results of Kandpal et al. [27] and Zhang et al. [17]. Zhang et al. found NiVSb to be nearly HMF with a moment of 1.90 μ_B.

For NiCrSb, resultant magnetic moment calculated is 3.01 μ_B which arises mainly from the exchange splitting energy of Cr-3d state electrons. The observed magnetic moments are compared with the results of Zhang et al. [16] and Li and Jin [18]. The effective moment and DOS plot confirms the stronger evidence of HMF.

For NiMnSb, resultant magnetic moment is found to be 3.99 μ_B which arises mainly from the exchange splitting energy of Mn-3d

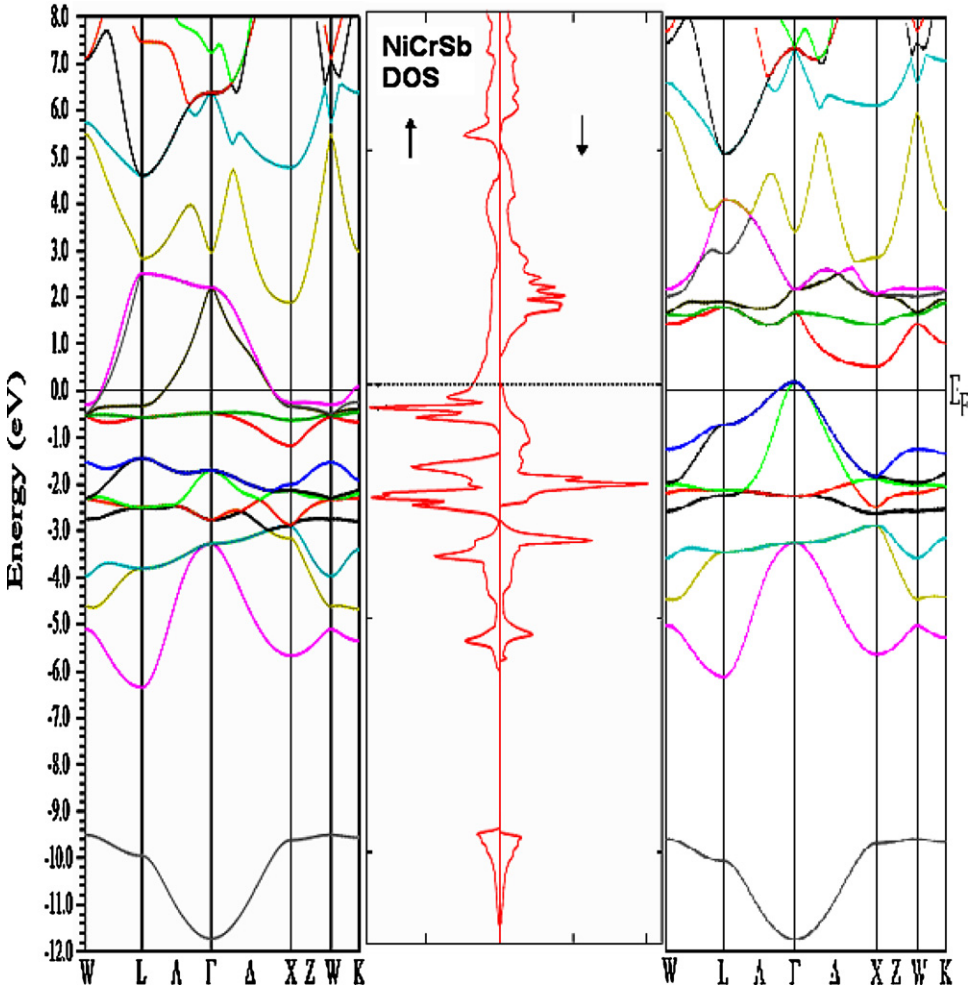

Fig. 9. Band structure in spin-up (left), spin-down (right) and DOS (middle) plots for NiCrSb. The horizontal line on the plot corresponds to the Fermi level.

state electrons. The contribution due to Ni and Sb atom is negligible. Although the moment is contributed by the Ni atoms but its contribution to the total moments is negligible. This is because the exchange splitting between spin-up and spin-down states of Ni-e_g (t_{2g}) are cancelling each other. Our observation shows that the magnetic moments of NiMnSb agrees well with the results obtained by others [27,30–32] and confirms the HMF nature.

3.4. Band structures

In the HMF compounds, the gap in spin-down channel basically arises from covalent hybridization between the lower energy 3d states of high-valent transition metal like Ni and the higher-energy 3d states of lower-valent transition metals like Ti, V, Cr or Mn leading to the formation of bonding and antibonding bands with a gap in between [33]. For these reasons the 5-sp elements like Sb plays an important role in the existence of Heusler compounds with a gap at the Fermi level.

The electronic band structure plots of NiTiSb, NiVSb, NiCrSb and NiMnSb in spin-up and spin-down configurations are shown in Figs. 7–10 along various symmetry directions. The total DOS is also included between spin-up and spin-down band structure plot for comparison. Thicker bands observed at various energy sites in the band structure supports the peaks in the DOS plots. As shown in Fig. 7, we observe that the energy bands were found to overlap each other except near E_F in both spin channels. A virtual energy-gap of 0.53 eV was noted below E_F due to Ni-3d and Sb-5p interactions in both spins. In the conduction region more dispersive bands were observed which are contributed dominantly by the Ti-d state electrons. From the band structure and DOS calculations, NiTiSb is found to act as a semiconductor while the exchange contribution due to Ti-d electrons makes NiTiSb a ferromagnet. The observed result is in close agreement with the result provided by Tobola et al. [25] using KKR method, while contradicts with the result of Larson et al. [34] in which they found that NiTiSb is a metal in its lowest-energy configuration.

From the band structure and DOS plots of NiVSb, NiCrSb and NiMnSb, we observe metallic behavior with Fermi cut-off in spin-up channel and semi-conducting gap in spin-down channel. Spin-up band structure is found to replicate with the energy bands which correspond to the sharp DOS peaks in terms of multiple interacting bands at the corresponding energy level. In spin-down band structure, we find an indirect band gap at E_F in which maximum of the valence band lies at the symmetry point Γ and the minimum of the conduction band lies at symmetry point X. The contributions to the energy bands is mainly due to the partial DOS contributions from Sb-sp, Ni-d and X-d electrons in both spin channels. Indirect band gap of 0.49 eV, 0.38 eV and 0.48 eV were observed for NiVSb, NiCrSb and NiMnSb respectively and are compared in Table 3. Strong indication of HMF is displayed by the spin-down band-gap at E_F as suggested by the DOS plots with an integral magnetic moment.

The band structure plots of NiMnSb as shown in Fig. 10 supports the DOS findings both in spin-up and spin-down channel. From the partial DOS plot (Fig. 6) and band structure it can be observed that

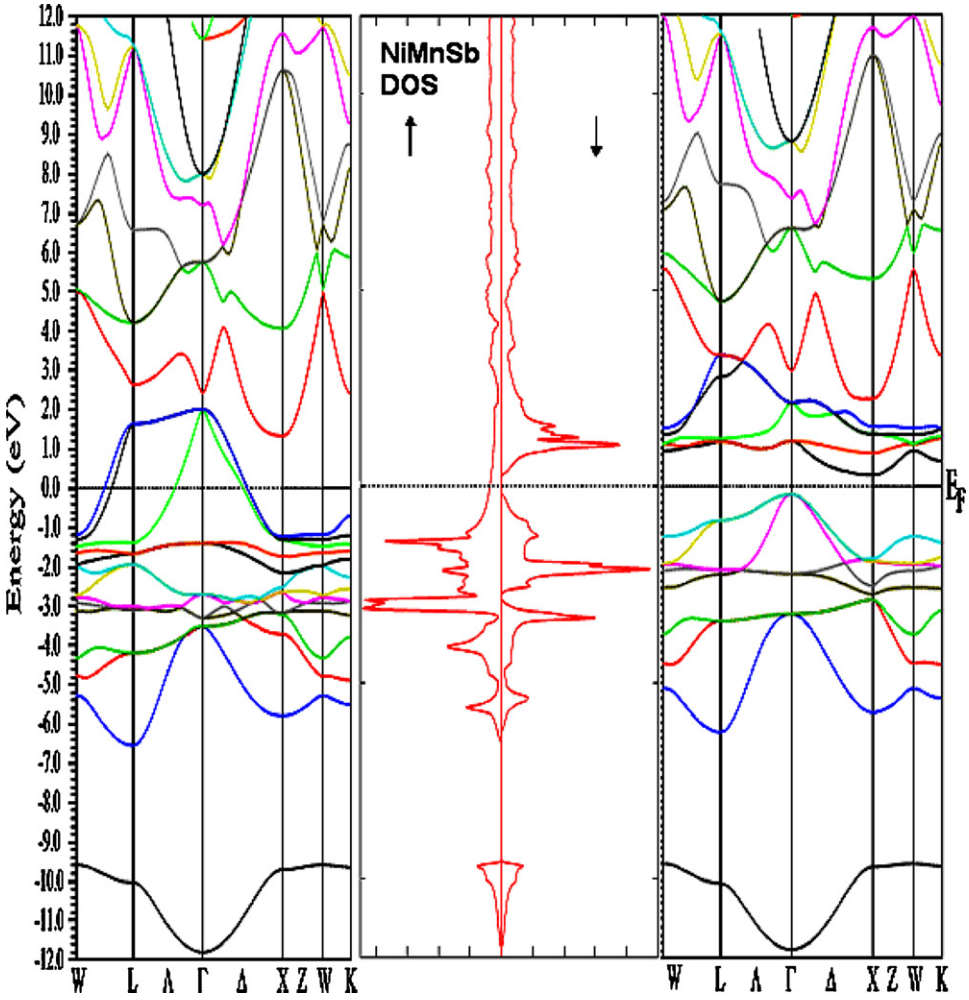

Fig. 10. Band structure in spin-up (left), spin-down (right) and DOS (middle) plots for NiMnSb. The horizontal line on the plot corresponds to the Fermi level.

the spin-up Mn-d and Ni-d states are located at the same energy sites, while spin-down bands are separated due to the Mn exchange splitting. The top of the valence bands is formed by the Mn t_{2g}, Sb p and Ni t_{2g} orbitals, while the bottom of the conduction bands are due to Mn e_g and t_{2g} states in spin-down. This means that the large Mn spin-splitting and Sb-mediated indirect Mn–Ni interactions are responsible for the formation of the HM gap [35].

4. Conclusions

First principles FP-LAPW method within GGA is carried out to calculate the electronic and magnetic properties of NiXSb in zinc-blende structure. The optimized lattice parameters of NiXSb are used for the calculations of DOS, magnetic moments and band structure. From the observed results, it is found that NiVSb, NiCrSb and NiMnSb are HMF while NiTiSb shows the possibility of HMF. The observed results are found to agree well with the earlier experimental and theoretical results. The DOS of different systems under study are mainly characterized by exchange splitting of 3d states of X atoms which leads to larger localized spin moments at the Ti, V, Cr or Mn sites. From the DOS and band-structure calculations, ferromagnetism is of itinerant and highly spin-polarized type. The calculated magnitude of the energy gaps in spin-down configuration for NiTiSb, NiVSb, NiCrSb and NiMnSb are 0.53 eV, 0.49 eV, 0.38 eV and 0.48 eV respectively along the symmetry direction Γ-X. The effective moments are calculated to be 0.35 μ_B, 1.995 μ_B, 3.01 μ_B and 3.99 μ_B respectively for NiTiSb, NiVSb, NiCrSb and NiMnSb. An apparent shift of the band gap towards the conduction region was found when compared with others result.

References

[1] R.A. de Groot, K.H.J. Bushow, J. Magn. Magn. Mater. 54–57 (1986) 1377–1380.
[2] S.W. Robey, L.T. Hudson, R.L. Kurtz, Phys. Rev. B 46 (1992) 11697–11704.
[3] M.V. Yablonskikh, Yu.M. Yarmoshenko, V.I. Grebennikov, E.Z. Kurmaev, S.M. Butorin, L.C. Duda, J. Nordgren, S. Plogmann, M. Neumann, Phys. Rev. B 63 (2001) 235117–235126.
[4] J.S. Moodera, L.R. Kinder, T.M. Wong, R. Merservey, Phys. Rev. Lett. 74 (1995) 3273–3276.
[5] S.S.P. Parkin, K.P. Roche, M.G. Samant, P.M. Rice, R.B. Beyers, R.E. Scheuerlein, E.J.O. Sullivan, S.L. Brown, J. Bucchigano, D.W. Abraham, Lu. Yu, M. Rooks, P.L. Trouilloud, R.A. Wanner, W.J. Gallagher, J. Appl. Phys. 85 (1999) 5828–5833.
[6] J. Kubler, Physica B+C 127 (1984) 257–263.
[7] Hyunjin Ko, Structural and electronic investigations of complex intermetallic compounds, Ph.D. Thesis, Iowa State University, Ames, Iowa (2008).
[8] D. Jung, H.-J. Koo, M.-H. Whangbo, D. Jung, H.-J. Koo, M.-H. Whangbo, J. Mol. Struct. (THEOCHEM) 527 (2000) 113–119.
[9] E.C. Stoner, Proc. R. Soc. Lond. 165 (1938) 372–414.
[10] I. Galanakis, P.H. Dederichs, N. Papanikolou, Phys. Rev. B 66 (2002) 174429–174437.
[11] J. Pierre, R.V. Skolozdra, J. Tobola, S. Kaprzyk, C. Hordequin, M.A. Kouacou, I. Karla, R. Currat, E. Leliévre-Berna, J. Alloys Compd. 262–263 (1997) 101–107.
[12] J. Tabola, J. Pierre, J. Alloys Compd. 296 (2000) 243–252.
[13] S. Ogut, K.M. Rabe, Phys. Rev. B 51 (1995) 10443–10453.
[14] B.R.K. Nanda, I. Dasgupta, J. Phys.: Condens. Matter 15 (2003) 7307–7323.
[15] B.R.K. Nanda, I. Dasgupta, J. Phys.: Condens. Matter 17 (2005) 5037–5048.
[16] M. Zhang, X. Dai, H. Hu, G. Liu, Y. Cui, Z. Liu, J. Chen, J. Wang, G. Wu, J. Phys.: Condens. Matter 15 (2003) 7891–7899.
[17] M. Zhang, Z.H. Liu, H.N. Hu, G.D. Liu, Y.T. Cui, G.H. Wu, E. Bruck, F.R. de Boer, Y.X. Li, J. Appl. Phys. 95 (2004) 7219–7221.
[18] G.-N. Li, Y.-J. Jin, Chin. Phys. Lett. 26 (2009) 1071010–1071014.

[19] W. Kohn, L.J. Sham, Phys. Rev. A 140 (1965) 1133–1138.
[20] P. Blaha, K. Schwarz, G.K.H. Madsen, D. Kvasnicka, J. Luitz, WIEN2k, An Augmented Plane Wave Plus Local Orbitals Program for Calculating Crystal Properties, Vienna University of Technology, Vienna, Austria, 2008.
[21] J.P. Perdew, S. Burke, M. Ernzerhof, Phys. Rev. Lett. 77 (1996) 3865–3868.
[22] F.D. Murnaghan, Proc. Natl. Acad. Sci. U.S.A. 30 (1944) 244–247.
[23] H.C. Kandpal, Computational studies on the structure and stabilities of magnetic inter-metallic compounds, Ph.D. Thesis, Institut für Anorganische und Analytische Chemie, (Johannes Gutenberg-Universität, Mainz, Germany).
[24] S. Ishida, T. Masaki, S. Fujii, S. Asano, Physica B: Condens. Matter 237–238 (1997) 363–364.
[25] J. Tobola, J. Pierre, S. Kaprzyk, R.V. Skolozdra, M.A. Kouacou, J. Phys.: Condens. Matter 10 (1998) 1013–1032.
[26] Sandeep, M.P. Ghimire, D.P. Rai, R.K. Thapa, Indian J. Phys., INJP-D-10-00340R1, in press.
[27] H.C. Kandpal, C. Felser, R. Seshadri, J. Phys. D: Appl. Phys. 39 (2006) 776–785.
[28] M.P. Ghimire, Sandeep, J. Maibam, D.P. Rai, R.K. Thapa, Conference on Theoretical Condensed Matter Physics-2011, Assam University, 3–5th February, 2011.
[29] P.H. Dederichs, I. Galanakis, Ph. Mavropoulos, J. Electron Microsc. 54 (2005) i53–i56.
[30] S.J. Youn, B.I. Min, Phys. Rev. B 51 (1995) 10436–10442.
[31] K.H.J. Buschow, P.G. van Engen, R. Jongebreur, J. Magn. Magn. Mater. 38 (1983) 1–22.
[32] I. Galanakis, Ph. Mavropoulos, J. Phys.: Condens. Matter 19 (2007) 315213–315220.
[33] M.P. Ghimire, Sandeep, R.K. Thapa, Mod. Phys. Lett. B 24 (2010) 2187–2193.
[34] P. Larson, S.D. Mahanti, M.G. Kanatzidis, Phys. Rev. B 62 (2000) 12754–12762.
[35] M.I. Katsnelson, V.Yu. Irkhin, L. Chioncel, A.I. Lichtenstein, R.A. de Groot, Rev. Mod. Phys. 80 (2008) 315–378.